

Spaser as Nanoscale Quantum Generator and Ultrafast Amplifier

Mark I. Stockman^{1,2,3}

¹ *Department of Physics and Astronomy, Georgia State University, Atlanta, Georgia 30303, USA*

² *Max Planck Institute for Quantum Optics, Hans-Kopfermann-Strasse 1, 85748 Garching, Germany*

³ *Ludwig Maximilian University Munich, Am Coulombwall 1, 85748 Garching, Germany**

(Dated: October 29, 2018)

Nanoplasmonics has recently experienced explosive development with many novel ideas and dramatic achievements in both fundamentals and applications. Among numerous applications of nanoplasmonics are efficient labels and sensitive assays for biomedical applications and defense, nanoantennas for solar cells and photodetectors, near-field scanning optical microscopes, surface-enhanced Raman scattering sensors, concentrators of laser energy for thermal-assisted ultradense magnetic recording, nanoplasmonic-assisted thermal cancer treatment, etc. One of the greatest obstacles to even greater fundamental development and wider applications on the nanoplasmonics is absence of an active element—an ultrafast nanoscale generator and amplifier of local fields—an optical counterpart of the MOSFET (metal-oxide-semiconductor field effect transistor). Here we show that the spaser, introduced and observed recently as a nanoscale counterpart of laser, can serve as such an active device. For the first time, we develop quantum theory of the spaser, find its threshold, intensity dependence, and spectrum. We show that the spaser can work in a regime as a nanoscale generator of local fields, and also a ultrafast, high-gain analog or logical amplifier, and memory cell. The spaser is shown to be three orders of magnitude faster than the MOSFET within the same geometric sizes on the order of 10 nm. These functions of spaser will further widen both the fundamental and applied horizons of nanoplasmonic science and technology. One may envision ultrafast (operation time less or on the order of 100 fs) nanoplasmonic chips with a high degree of integration where spasers communicate and control each other through their near fields or are connected with nanoplasmonic wires. These can perform ultrafast microprocessor functions. They can also be integrated with nano-photodetectors and nanosensors to form complex functions of intelligent ultrafast detection and sensing. In contrast to semiconductor technology, the spasers are based on metals and, therefore, are highly resistive to ionizing radiation, high temperatures and other adverse environments, with possible applications in nuclear industries and defense.

Nanoplasmonic phenomena (see, e.g., monograph Ref. 1) unfold on the spatial scale between the skin depth $l_s \approx 25$ nm (in noble metals) and the nonlocality radius $l_{nl} \sim v_F/\omega \sim 1$ nm, where v_F is the electron speed at the Fermi surface, and ω is optical frequency. Nanoplasmonics is ultrafast: the temporal scale of the nanoplasmonic phenomena is between the coherent time of hundred attoseconds defined by the inverse bandwidth of the plasmonic frequency range (between uv and mid ir for plasmonic metals and doped semiconductors)^{2,3} and the surface plasmon (SP) relaxation time $\gamma_p^{-1} \sim 10 - 100$ fs (for noble metals in the visible to near-ir frequency range).⁴ Not just a promise only any more,⁵ nanoplasmonics has delivered a number of important applications and effects with applied potentials: ultrasensing,⁶ scanning near-field optical microscopy,^{1,7} SP-enhanced photodetectors⁸ and thermally assisted magnetic recording,⁹ generation of extreme uv,¹⁰ biomedical tests,^{6,11} SP-assisted thermal cancer treatment,¹² and many others.

To continue its vigorous development, nanoplasmonics needs an active device – near-field generator and amplifier of nanolocalized optical fields, which has until recently been absent. Such a device in microelectronics – metal-oxide-semiconductor field-effect transistor (MOSFET)^{13,14} – has enabled all contemporary digital electronics, including computers and communications, and formed the present day technology as we know it. However, the MOSFET is limited by frequency to a

$\sim 10 - 100$ GHz band, which is already a limiting factor in the further technological development. Another limitation of the MOSFET is its high sensitivity to temperature, electric fields, and ionizing radiation, which limits its use in extreme environmental conditions and defense.

The required active element of nanoplasmonics is the SPASER (Surface Plasmon Amplification by Stimulated Emission of Radiation) that was introduced^{4,15} as a nanoscale quantum generator of nanolocalized, coherent, and intense optical fields. Here, for the first time, we build a quantum theory of the spaser that describes both its threshold behavior, stationary state, and ultrafast kinetics. We show that the spaser can function as a ultrafast nanoscale optical amplifier, which is of the same size ~ 10 nm as the MOSFET but can perform the same operations of amplification, generation and information storage by a factor of thousand faster. Importantly, the spaser is robust with respect to ionizing radiation, temperature, and microwave interference. Spasers can interact with each other and other elements of active nanoplasmonics in the near field, without emitting light, thus enabling technology to built large integrated circuits working in 10-100 THz bandwidth.

One may envision ultrafast (operation time less or on the order of 100 fs) nanoplasmonic chips with a high degree of integration where spasers communicate and control each other through their near fields or are connected with nanoplasmonic wires. These can perform ultrafast

microprocessor functions. They can also be integrated with nano-photodetectors and nanosensors to form complex functions of intelligent ultrafast detection and sensing. In contrast to semiconductor technology, the spasers are based on metals and, therefore, are highly resistive to ionizing radiation, high temperatures and other adverse environments, with possible applications in nuclear industries and defense. These functions of spaser will further widen both the fundamental and applied horizons of nanoplasmonics and, generally, science and technology.

I. INTRODUCTION

The spaser is a nanoplasmonic counterpart of the laser.^{4,15} The laser has two principal elements: resonator (or cavity) that supports photonic mode(s) and the gain (or active) medium that is population-inverted and supplies energy to the lasing mode(s). An inherent limitation of the laser is that the size of the cavity in the propagation direction is at least half wavelength and practically more than that even for the smallest laser fabricated.¹⁶ Therefore we proposed the spaser⁴ to overcome this limitation. The surface plasmon (SP) localization length is on the nanoscale¹⁷ and is only limited by the minimum inhomogeneity scale of the plasmonic metal and the non-locality radius¹⁸ l_{nl} .

In spaser, the SPs play the same role as photons in the laser because they have the same principal properties. (i) They are vector excitations: their field is the dielectric polarization. Thus, quantum mechanically, they possess spin 1 and, therefore, are bosons. (ii) Because they are due to the electric polarization (displacement of charges), they are electrically neutral excitations. (iii) The SPs are the most linear excitations of all known types in nature in the optical range of frequencies. This is due to the fact that they are very collective: the oscillator strength of the SPs is the total number of electrons in the nanosystem. This implies that a given electron possesses a very small fraction of the SP energy, which leads to the high harmonicity.

The resonator of a spaser is any metal nanoparticle whose size is between l_{nl} and l_s that supports a SP mode with required frequency ω_n . This metal nanoparticle should be surrounded by the gain medium that overlaps with the eigenmode spatially and whose emission line overlaps with the SP eigenmode spectrally.⁴ As an example, we consider a model of a nanoshell spaser,¹⁵ which is illustrated in Fig. 1. Panel (a) shows a silver nanoshell carrying a single SP (plasmon population number $N_n = 1$) in the dipole eigenmode. It is characterized by a uniform field inside the core and hot spots at the poles outside the shell with the maximum field reaching $\sim 10^6$ V/cm. Similarly, Fig. 1 (b) shows the quadrupole mode in the same nanoshell. In this case, the mode electric field is non-uniform, exhibiting hot spots of $\sim 1.5 \times 10^6$ V/cm of the modal electric field at the poles. These high values of the modal fields is the underlying

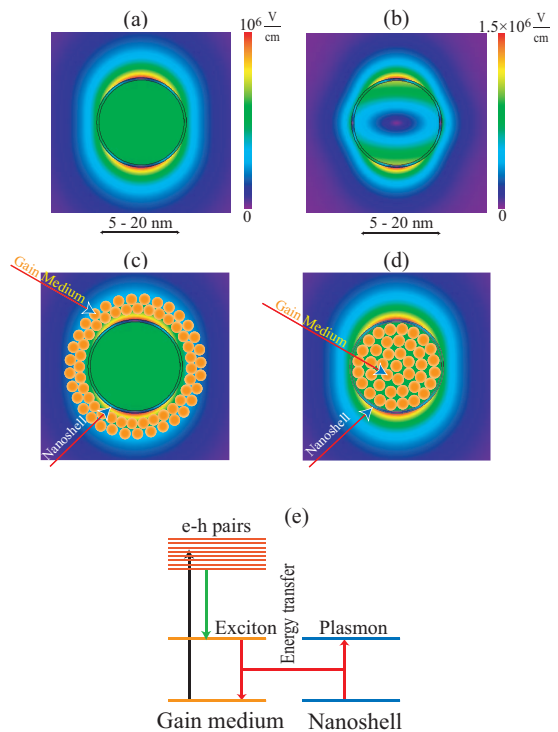


FIG. 1: Schematic of spaser geometry, local fields, and fundamental processes leading to spasing. (a) Nanoshell geometry and the local optical field distribution for one SP in an axially-symmetric dipole mode. The nanoshell has aspect ratio $\eta = 0.95$. The local field magnitude is color-coded by the scale bar in the right-hand side of the panel (b) The same as (a) but for a quadrupole mode. (c) Schematic of a nanoshell spaser where the gain medium is outside of the shell, on the background of the dipole-mode field. (d) The same as (c) but for the gain medium inside the shell. (e) Schematic of the spasing process. The gain medium is excited and population-inverted by an external source, as depicted by the black arrow, which produces electron-hole pairs in it. These pairs relax, as shown by the green arrow, to form the excitons. The excitons undergo decay in the ground state emitting SPs in the nanoshell. The plasmonic oscillations of the nanoshell stimulates this emission, supplying the feedback for the spaser action.

physical reason for very strong feedback in the spaser.

For the sake of numerical illustrations of our theory, we will use the dipole eigenmode [Fig. 1 (a)]. There are two basic ways to place the gain medium: (i) outside the nanoshell, as shown in panel (c), and (ii) in the core, as in panel (d). As we have verified, these two designs lead to comparable characteristics of the spaser. However, the placement of the gain medium inside the core illustrated in Fig. 1 (d) has a significant advantage because the hot spots of the local field are not covered by the gain medium and are spatially available for applications.

We have recently discussed the physical principles of the spasing¹⁵ but will briefly reiterate here for the sake of completeness and self-containment. The level diagram of the spaser gain medium and the plasmonic

metal nanoparticle is displayed in Fig. 1 (e) along with a schematic of the relevant energy transitions in the system. The gain medium chromophores may be semiconductor nanocrystals^{4,19} dye molecules,^{20,21} or electron-hole excitations of a bulk semiconductor.¹⁶ In all cases, we will use the semiconductor-science language of electrons and holes. The pump excites electron-hole pairs in the chromophores [Fig. 1 (e)], as indicated by the vertical black arrow, which relax to form excitons. The excitons constitute the two-level systems that are the donors of energy for the SP emission into the spasing mode. In vacuum, the excitons would recombine emitting photons. However, in the spaser geometry, the photoemission is strongly quenched due to the resonance energy transfer to the SP modes, as indicated by the red arrows in the panel. The plasmons in the spaser mode create the high local fields that excite the gain medium and stimulate more emission to this mode, which is the feedback mechanism. If this feedback is strong enough and the life time of the spaser SP mode is long enough, then an instability develops leading to the avalanche of the SP emission in the spasing mode and spontaneous symmetry breaking, establishing the phase coherence of the spasing state. This can be called a nonequilibrium phase transition, as in the physics of lasing.

After the original theoretical proposal and prediction of the spaser,⁴ there has been an active development in this field, both theoretical and experimental. We comment below in the next two paragraphs only on some representative publications. Regarding theoretical developments, a nanolens spaser has been proposed,²² which possesses a nanofocus (“the hottest spot”) the local fields. In Refs. 4,22, only the necessary condition of spasing has been established on the basis of the perturbation theory. There have been attempts to describe the spaser (or, “nanolaser” as sometimes it is called) on the basis of linear electrodynamics considering the gain medium as a dielectric with a negative imaginary part of the permittivity – see, e.g., Refs. 23,24,25. Such electrodynamic approaches do not take into account the nature of the spasing as the spontaneous symmetry breaking. This leads to principal differences of their results from ours as we discuss below in this paper, in particular, in Sec.IIB in connection with Fig. 2. There have also been theoretical proposals of a magnetic resonance nanolasers (which can be called magnetic spasers).^{26,27} A significant theoretical development has been a proposal of the lasing spaser,²⁸ which is made of a plane array of spasers.

There has been a vigorous experimental quest toward the spaser. The stimulated emission of surface plasmon polaritons (SPPs) has been observed in a proof-of-principle experiment using pumped dye molecules as an active medium.²⁰ There have also been later experiments that demonstrated strong stimulated emission compensating a significant part of the SPP loss^{21,29,30,31} As a step toward the lasing spaser, the first experimental demonstration has been reported of compensating Joule losses in a metallic photonic metamaterial using opti-

cally pumped PbS semiconductor quantum dots.¹⁹ An electrically-pumped nanolaser with semiconductor gain medium has been demonstrated¹⁶ where the lasing mode has a significant SPP content. There have also been experimental investigations reporting the stimulated emission effects of SPs in plasmonic metal nanoparticles surrounded by gain media with dye molecules.^{32,33}

There have been reports that the spaser has been experimentally observed.^{34,35,36} This spaser is a gold nanosphere of radius 7 nm surrounded by a dielectric shell of radius ~ 20 nm containing dye molecules. Under nanosecond excitation, this spaser develops a relatively narrow-spectrum and intense emission that exhibits a threshold. The observed characteristics of spaser are qualitatively very close to the corresponding theoretical results obtained below in Sec. II A.

II. SPASER IN MODE OF CONTINUOUS WAVE NANOSCALE QUANTUM GENERATOR

A. Theory of Spaser in Stationary Regime

Physically, the spaser action is a result of spontaneous symmetry breaking when the phase of the coherent SP field is established from the spontaneous noise. Mathematically, the spaser is described by homogeneous differential Eqs. (11)-(13) derived and solved in Sec. VI. These equations become homogeneous algebraic equations for the stationary (CW) case. These equations always have a trivial, zero solution. However, when their determinant vanishes, they also possess a nontrivial solution describing spasing, whose condition is

$$\begin{aligned} & (\omega_s - \omega_n + i\gamma_n)^{-1} \times \\ & (\omega_s - \omega_{21} + i\Gamma_{12})^{-1} \sum_p \left| \tilde{\Omega}_{12}^{(p)} \right|^2 n_{21}^{(p)} = -1, \end{aligned} \quad (1)$$

where ω_s is the spasing frequency, $\tilde{\Omega}_{12}^{(p)} = -A_n \mathbf{d}_{12}^{(p)} \nabla \varphi_n(\mathbf{r}_p) / \hbar$ is the single-plasmon Rabi frequency, $\mathbf{d}_{12}^{(p)}$ is the transition dipole moment of a p th chromophore, $\varphi_n(\mathbf{r}_p)$ is the electric potential of the spasing mode at the position this chromophore, γ_n is the decay rate of the SP mode,⁴ Γ_{12} is the width and ω_{21} is the frequency of the spasing transition in the chromophores. Here A_n is the amplitude of the quantized SP field⁴: $A_n = (4\pi\hbar s_n / \varepsilon_d s'_n)^{1/2}$, $s_n = s(\omega_n)$, $s'_n = \partial s(\omega_n) / \partial \omega_n$, where $s(\omega) = [1 - \varepsilon_m(\omega) / \varepsilon_d]^{-1}$ is Bergman’s spectral parameter with $\varepsilon_m(\omega)$ as the permittivity of the metal and ε_d that of the surrounding dielectric. The population inversion of a p th chromophore $n_{21}^{(p)}$ is explicitly expressed as

$$\begin{aligned} n_{21}^{(p)} = & (g - \gamma_2) \times \\ & \left\{ g + \gamma_2 + 4 \left| \Omega_{12}^{(p)} \right|^2 / \left[(\omega_s - \omega_{21})^2 + \Gamma_{12}^2 \right] \right\}^{-1}, \end{aligned} \quad (2)$$

where $\Omega_{12}^{(p)} = \tilde{\Omega}_{12}^{(p)} \sqrt{N_n}$ is the Rabi frequency in a state with containing N_n of SP quanta, g is the pumping rate per a chromophore, and γ_2 is the decay rate of the upper spasing level population.

From the imaginary part of Eq. (2) we immediately find the spasing frequency

$$\omega_s = (\gamma_n \omega_{21} + \Gamma_{12} \omega_n) / (\gamma_n + \Gamma_{12}) , \quad (3)$$

which generally does not coincide with either the gain transition frequency ω_{21} or the SP frequency ω_n , but is between them (this is a frequency walk-off phenomenon similar to that of laser physics). Substituting Eq. (3) back to Eqs. (2)- (3), we obtain a system of equations

$$\begin{aligned} & \frac{(\gamma_n + \Gamma_{12})^2}{\gamma_n \Gamma_{12} \left[(\omega_{21} - \omega_n)^2 + (\Gamma_{12} + \gamma_n)^2 \right]} \times \quad (4) \\ & \sum_p \left| \tilde{\Omega}_{12}^{(p)} \right|^2 n_{21}^{(p)} = 1 , \\ & n_{21}^{(p)} = (g - \gamma_2) \times \quad (5) \\ & \left[g + \gamma_2 + \frac{4 \left| \Omega_{12}^{(p)} \right|^2 \times (\Gamma_{12} + \gamma_n)}{(\omega_{21} - \omega_n)^2 + (\Gamma_{12} + \gamma_n)^2} \right]^{-1} . \end{aligned}$$

This system defines the stationary number of SPs per spasing mode N_n , which enters the equations via the Rabi frequency $\Omega_{12}^{(p)}$.

Since $n_{21}^{(p)} \leq 1$, from Eq. (5) we immediately obtain a necessary condition of the existence of spasing,

$$\frac{(\gamma_n + \Gamma_{12})^2}{\gamma_n \Gamma_{12} \left[(\omega_{21} - \omega_n)^2 + (\Gamma_{12} + \gamma_n)^2 \right]} \sum_p \left| \tilde{\Omega}_{12}^{(p)} \right|^2 \geq 1 . \quad (6)$$

This expression is fully consistent with Ref. 4. The following order of magnitude estimate of this spasing condition has a transparent physical meaning and is of heuristic value,

$$\frac{d_{12}^2 Q N_c}{\hbar \Gamma_{12} V_n} \gtrsim 1 , \quad (7)$$

where $Q = \omega / \gamma_n$ is the quality factor of SPs, V_n is the volume of the spasing SP mode, and N_c is the of number of the gain medium chromophores within this volume. Deriving this estimate, we have neglected the detuning, i.e., set $\omega_{21} - \omega_n = 0$. It follows from Eq. (7) that for the existence of spasing it is beneficial to have a high quality factor Q , a high density of the chromophores, and a large transition dipole (oscillator strength) of the chromophore transition. The small modal volume V_n (at a given number of the chromophores N_c) is beneficial for this spasing condition: physically, it implies strong feedback in the spaser. Note that for the given density of the chromophores $\rho_c = N_c / V_n$, this spasing condition does not explicitly depend on the spaser size, which opens up a possibility of spasers of a very small size limited from the bottom by only the nonlocality radius $l_{nl} \sim 1$ nm.

B. Kinetics of CW Spaser

The "spasing curve", i.e., the dependence of the coherent SP population N_n on the excitation rate g , obtained by solving Eqs. (5) and (6) is shown in Fig. 2 (a) for four types of the silver nanoshells with the frequencies of the spasing dipole modes as indicated, which are in the range from near ir ($\hbar\omega_s = 1.2$ eV) to mid visible ($\hbar\omega_s = 2.2$ eV). In all cases, there is a threshold of the spasing with the excitation rate $g_{th} \sim 10^{12}$ s⁻¹. Soon after the threshold, the dependence $N_n(g)$ becomes linear, which means that every quantum of excitation added to the active medium with a high probability is stimulated to be emitted as a SP, adding to the coherent SP population. While this is similar to conventional lasers, there is a dramatic difference of the spaser. In the lasers a similar relative rate of the stimulated emission is achieved at a photon population of $\sim 10^{18} - 10^{20}$, while in the spaser the SP population is $N_n \lesssim 100$. This is due to much stronger feedback due to much smaller modal volume V_n – see discussion of Eq. (7).

The population inversion number n_{21} as a function of the excitation rate g is displayed in Fig. 2 (b) for the same set of frequencies (and with the same color coding) as in panel (a). Before the spasing threshold, n_{21} increases with g to become positive just before the onset of the population inversion. For higher g , the spasing threshold is reached, after which n_{21} becomes constant (the population pinning). The pinned levels of the inversion are very low, $n_{21} \sim 0.01$, which is due to the very strong feedback in the spaser.

The spectral width Γ_s of the spaser generation, as defined by Eq. (15), is displayed in Fig. 2 (c) as a function of the pumping rate g . At the threshold, this width is that of the SP line γ_n but for stronger pumping, as the SPs accumulate in the spasing mode, it decreases $\propto N_n^{-1}$, as given by Eq. (15). This decrease of Γ_s reflects the higher coherence of the spasing state with the increased number of SP quanta and, correspondingly, lower quantum fluctuations.

The developed spasing in a dipole SP mode will show itself in the far field as an anomalously narrow and intense radiation line. The shape and magnitude of this line in relation to the lines of the spontaneous fluorescence of the isolated gain medium and its SP-enhanced fluorescence line in the spaser is illustrated in Figs. 2 (d)-(f). Note that for the system under consideration, there is a 20 meV red shift of the gain medium fluorescence with respect to the SP line center. It is chosen so to illustrate the spectral walk-off of the spaser line. For one percent in the excitation rate above the threshold of spasing [panel (d)], a broad spasing line (red color) appears comparable in intensity to the SP-enhanced spontaneous fluorescence line (blue color). The width of this spasing line is approximately the same as of the fluorescence, but its position is shifted appreciably (spectral walk-off) toward the isolated gain medium line (green color). For the pumping twice more intense [panel (e)], the spaser-

line radiation dominates, but its width is still close to that of the SP line due to significant quantum fluctuations of the spasing state phase. Only when the pumping rate is an order of magnitude above the threshold, the spaser line strongly narrows [panel (f)], and it also completely dominates the spectrum of the radiation. This is a regime of small quantum fluctuations, which is desired in applications.

These results are different in the most dramatic way from previous models based on the consideration of the spaser as a gain medium that has negative imaginary part of its permittivity, plus lossy metal nanosystem, described purely electro-dynamically.^{24,25} For instance, in a toy model²⁴, the width of the resonance line tends to zero at the threshold of spasing and then broadens up again. This distinction of the present theory is in the nature of the spasing as a spontaneous symmetry breaking (nonequilibrium phase transition) influenced by the phase relaxation due to the spontaneous emission into the spasing mode.

III. BISTABLE SPASER: QUANTUM LOGICAL AMPLIFIER AND MEMORY NANODEVICE

Logical amplifiers in microelectronics are MOSFET-based bistable devices that have two stable states describing logical 1 and 0. Their output “logical” level changes when the input exceeds a certain threshold value. They are also used to compensate losses in the transmission nanowires, bringing weakened signals back to the standard (logical) levels. Below we show that the spaser can operate as a logical amplifier that is faster than the corresponding MOSFET-based devices by orders of magnitude.

Generally, bistability is a result of nonlinearity in the system. We examine below the bistability in the spaser where the nonlinearity is due to the presence of a saturable absorber. Such an absorber is a chromophore whose absorption overlaps with the spasing line, but which does not absorb the radiation pumping the spaser. Formally, it is described by Eqs. (5), (6) where the pumping rate $g = 0$ for the index p corresponding to the saturable absorber. We will assume that this absorber is distributed in the space the same way as the gain chromophores but with a different density ρ_a .

Results of a numerical solution of Eqs. (5), (6) for different values of ρ_a relatively to the concentration ρ of the gain medium chromophores are shown in Fig. 3. Panel (a) displays dependence of the SP population number N_n in the spasing mode on the pumping rate g , and the panel (b) shows the corresponding dependence of the population inversion n_{21} of the gain medium. We note first that there always exists also a trivial, non-spasing solution $N_n = 0$. For values of g above critical (depending on ρ_a), there are also nontrivial solutions. For $\rho_a > 10^{-3}\rho$, these nontrivial solutions consist of two branches: high- N_n and low- N_n . Note that the high- N_n branch in panel

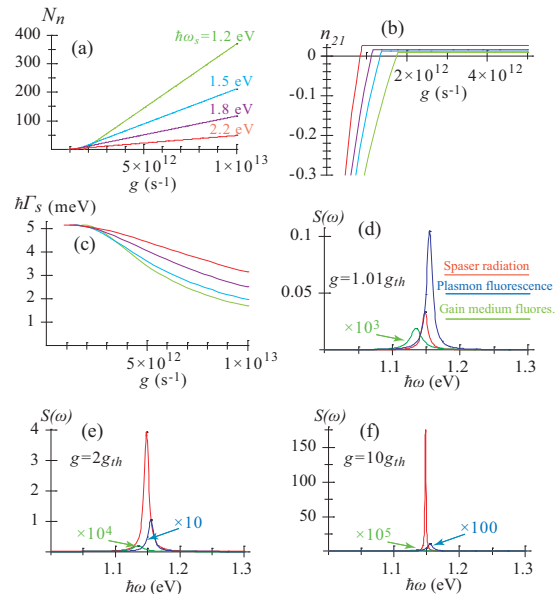


FIG. 2: Spaser SP population and spectral characteristics in the stationary state. The computations are done for a silver nanoshell with the external radius $R_2 = 12$ nm; the detuning of the gain medium from the spasing SP mode is $\hbar(\omega_{21} - \omega_n) = -0.02$ eV. The other parameters are indicated in Sec. VI. (a) Number N_n of plasmons per spasing mode as a function of the excitation rate g (per one chromophore of the gain medium). Computations are done for the dipole eigenmode with the spasing frequencies ω_s as indicated, which were chosen by the corresponding adjustment of the nanoshell aspect ratio. (b) population inversion n_{12} as a function of the pumping rate g . The color coding of the lines is the same as in panel (a). (c) The spectral width Γ_s of the spasing line (expressed as $\hbar\Gamma_s$ in meV) as a function of the pumping rate g . The color coding of the lines is the same as in panel (a). (d)-(f) Spectra of the spaser for the pumping rates g expressed in the units of the threshold rate g_{th} , as indicated in the panels. The curves are color coded and scaled as indicated.

(a) corresponds to the low- n_{21} branch in panel (b), and *vice versa*.

Thus it appears that there is a tri-stability. However, this impression is incorrect. The lower branches in Fig. 3 (a) [and, correspondingly, the upper branches in panel (b)] describe unstable solutions that are not realizable physically. This can be understood already from the fact that along these branches the SP population decreases with increasing pumping, which is completely unphysical.

It is a bistability, not the tri-stability, which takes place in actuality. This is illustrated in Figs. 3 (c) and (d) obtained by isolating the stable branches of the solutions. As one can see, with an increase of the pumping rate g , the solutions appear at critical pumping rates that increase with the saturable absorber concentration ρ_a . As the critical g for a given ρ_a is reached, the nonzero- N_n branch appears with a discontinuity. Both the $N_n = 0$ and $N_n > 0$ branches are stable and can keep their states indefinitely. The transition between these two stable states can be induced by either adding SP quanta to or

removing them from the spasing mode, as illustrated by arrows for $\rho_a = 3\rho$. This shows that a bistable spaser with a saturable absorber can serve functions of both a nanoscopic memory cell and a logical amplifier. The dynamics of such an amplifier is femtosecond and its gain coefficient is rather high (~ 50), as we will show below in Sec. IV.

In the bistable case there is no perfect pinning of the population inversion n_{21} , as Fig. 3 (d) shows. When the pumping rate g is increased, the system moves along the stable no-spasing ($N_n = 0$) solution denoted by the black line, where the inversion n_{21} significantly overshoots its values for the spasing branches (colored lines). When the transition to spasing occurs, induced, e.g., by an injection of SPs quanta, its is always discontinuous, as the vertical arrows indicate. Along the spasing ($N_n > 0$) branches (colored lines), the inversion counterintuitively decreases with increased pumping due to the stimulated emission. This behavior is in a sharp contrast to the monostable spaser (without a saturable absorber) – cf. Fig. 2 – where the perfect pinning takes place after the onset of the spasing.

IV. ULTRAFAST DYNAMICS OF SPASER

It is of the utmost importance how fast the spaser operates. As we show below in this Section, the spaser is indeed an ultrafast nanodevice with typical operating times on the order of 100 fs, which makes it most suitable for ultrahigh-speed nanophotonics operating in the bandwidth of ~ 10 THz.

The temporal behavior of the spaser can be found by direct numerical solution of Eqs. (11)-(13). The solution is facilitated by the fact in the model under consideration all the chromophores experience the same local field inside the nanoshell, and there are only two types of such chromophores: belonging to the active medium and the saturable absorber, if it is present.

The dynamical behavior of the monostable spaser (without a saturable absorber) is illustrated in Figs. 4 (a), (b). It is assumed that the gain medium pumping starts with the rate of $g = 5 \times 10^{12} \text{ s}^{-1}$ at the moment of time $t = 0$. As we see, the spaser, which starts from an arbitrary initial population N_n , rather rapidly, within a few hundred femtoseconds approaches the same stationary (“logical”) level. At this level, an SP population of $N_n = 67$ is established, while the inversion is pinned at a low level of $n_{21} = 0.02$. On the way to this stationary state, the spaser experiences relaxation oscillations in both the SP numbers and inversion, which, understandably, oscillate out of phase.

A radically different dynamics takes place in the presence of the saturable absorber. We show in Figs. 4 (c), (d) the dynamics of the spaser with the concentration of the saturable absorber $\rho_a = 0.66\rho$ and stationary pumping at the level $g = 5 \times 10^{12} \text{ s}^{-1}$. For the initial population $N_n > 1$, the spaser undergoes a few relaxation

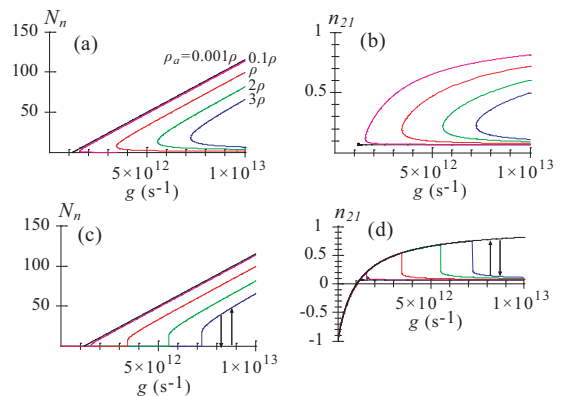


FIG. 3: Bistability in spaser with saturable absorber in a stationary spasing state. (a) Dependence of the SP population number N_n in the spasing mode on the pumping rate g for different concentrations ρ_a of the saturable absorber. The curves are color coded corresponding to ρ_a shown in the units of the concentration ρ of the active medium chromophores. The black curve shows the threshold curve (separatrix) between the bistable and uniquely stable solutions. (b) The dependence of the population inversion n_{21} on the pumping rate g for the spasing states. The color coding is the same as in panel (a). Note that the lower branches of the curves in this panel correspond to the upper ones in panel (a) and vice versa. (c) The physical bistable behavior of spaser: dependence of the SP population N_n on the pumping rate g . One of the two solutions is $N_n = 0$ (coincides with the horizontal axis). The family of the spasing solutions is shown by colored curves whose coding coincides with that in panel (a). The vertical arrows illustrate transitions between the two stable states for $\rho_a = 3\rho$. The black line separates the region of the uniquely stable and bistable solutions. (d) Physical solutions for population inversion n_{21} corresponding to those for the SP population in panel (c). The black curve starting with $n_{21} = -1$ shows one of the trivial stable solutions corresponding to the absence of spasing ($N_n = 0$). This curve is the same for any ρ_a . The color curves, coded the same way as in panel (a), show the nontrivial spasing solutions corresponding to the similarly colored curves in panel (c). The arrows also correspond to those in panel (c).

oscillations with a ~ 100 fs period, rapidly reaching the stationary level $N_n^{(1)} \approx 60$, which is slightly lower than in the absence of the absorber [cf. panels (a) and (b)], and stays at this stationary (logical) level indefinitely. Likewise, at a small initial population, $N_n < 1$, the spaser rapidly reaches the zero level, $N_n = 0$ and, again, stays at this other stable logical level indefinitely long. There is a separatrix that divides these two attractors (stable logical states) at the initial value of $N_n^{(s)} \approx 1$ (for the present set of parameters). For an initial condition close to this critical value, the spaser is undergoing a relatively long evolution and eventually falls into one of the two stable, logical levels of excitation (see the black and light-blue curves). The dynamics close to the separatrix is always longer, with the relaxation time diverging at the separatrix proper. This is a typical behavior of a

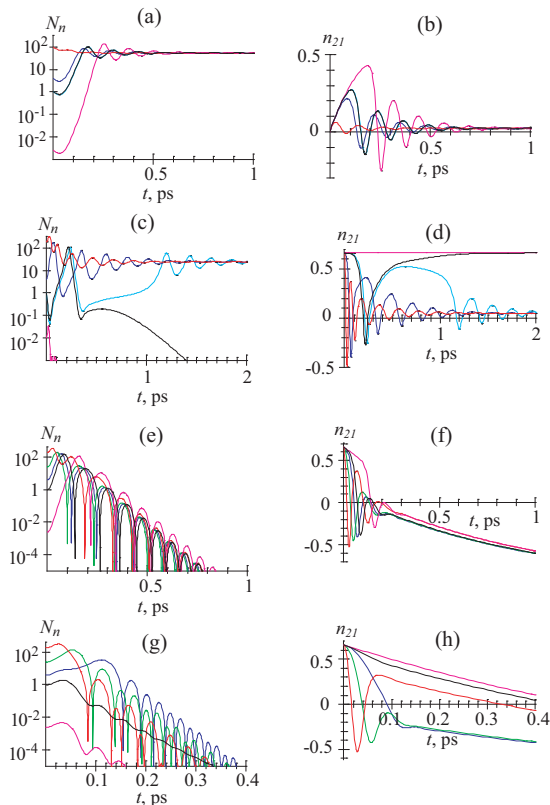


FIG. 4: Ultrafast kinetics of the spaser. (a) For a mono-stable spaser (without a saturable absorber), dependence of the SP population in the spasing mode N_n on the time t after the start of the gain medium pumping. The color-coded curves correspond to the initial conditions with the different initial SP populations, as shown in the graphs. (b) The same as (a) but for the temporal behavior of the population inversion n_{21} . (c) Temporal kinetics of the coherent SP population N_n in a bistable spaser with the saturable absorber in concentration $\rho_a = 0.66\rho$. Spaser is stationary pumped at a rate of $g = 5 \times 10^{12} \text{ s}^{-1}$. The colored curves correspond to the different initial SP populations as shown in the graphs. (d) The same as (c) but for the corresponding population inversion n_{21} . (e) Dynamics of a mono-stable spaser (no saturable absorber) with the saturating pulse pumping at the initial moment only. Coherent SP population N_n is displayed as a function of time t . Different initial populations are indicated by color-coded curves. (f) The same as (e) but for the corresponding population inversion n_{21} . (g) Dynamics of the bistable spaser with the concentration of the saturable absorber $\rho_a = 0.66\rho$ and pulsed pumping at the initial moment only. The coherent SP population N_n is displayed as a function of time t . The color-coded curves correspond to different initial N_n . (h) The same as in panel (g) but for the corresponding population inversion.

logical amplifier whose gain (amplification coefficient) is $N_n^{(1)}/N_n^{(s)} \approx 60$, which is very large, more that is required in microelectronics for a logical circuitry to function. Thus the spaser can make a high-gain, ~ 10 THz-bandwidth logical amplifier or dynamical memory cell with excellent prospects of applications.

We note that the spaser dynamics described above in the previous paragraph confirms that the spaser can stay only in one of the two states corresponding to the stable branches that we indicated in Figs. 3 (c), (d) (see also the corresponding discussion). The spaser never persists at or near the unstable branches of the stationary solutions, which we discussed in conjunction with Figs. 3 (a), (b). As a general comment, the bistability in the spaser with the saturable absorber is reminiscent of the intrusion phenomena of the first-order phase transition, while the behavior of the monostable spaser (without a saturable absorber) reminds that of a system with the second-order phase transition.

The spaser as a *pulse* amplifier is of a particular interest. In this case, the spaser gain-medium population is inverted to saturation with a short pump pulse, after which some number of plasmons can be injected (say, by an external nanoplasmonic circuitry). In response, the spaser should produce, in a controllable way, an amplified pulse of the SP excitation. Such a function of the spaser is illustrated in Figs. 4 (e)-(h).

We start with the spaser without a saturable absorber whose behavior is shown in Figs. 4 (e), (f). As we see from panel (e), independently from the initial number of SPs, the spaser always responds with generating a series of SP pulses, of which only the first pulse is large (at or above the logical level of $N_n \sim 100$). The underlying mechanism of such a response is the rapid depletion of the inversion seen in panel (f), where energy is dissipated in the metal of the spaser. The characteristic duration of the SP pulse ~ 100 fs is also defined by this depletion. This time is much shorter than the spontaneous decay time of the gain medium. This acceleration is due to the stimulated emission of the SPs. The discussion of this paragraph implies that the spaser is a potent femtosecond-pulse amplifier of the nanoscale fields.

Finally, the behavior of the bistable spaser with the saturable absorber as a pulse logical amplifier is illustrated in Figs. 4 (g), (h). In this case, there is a critical level of the initial population $N_n \approx 1$, at or below which the system rapidly relaxes to the zero level without producing an amplified pulse. For $N_n \geq 2$, a short amplified pulse within ~ 100 fs follows whose amplitude is at or above the logical level of $N_n \approx 50$. This demonstrated the spaser capability as a ultrafast-pulse optical logical amplifier with the gain ≈ 50 and the bandwidth ~ 10 THz. Taking into account that the produced local fields are concentrated within a few tens of nanometers, these are parameters that bear promise of many applications in the fundamental science and coming digital and analog technologies.

V. DISCUSSION AND CONCLUSIONS

Despite its many achievements and applications, as outlined in the Introduction to this article, nanoplasmonics still profoundly lacks the most important, ac-

tive element: an ultrafast generator and amplifier of nanolocalized optical fields. If one draws an analogy between nanoplasmonics and microelectronics, then the nanoplasmonics today would be similar to the microelectronics without the transistor. It is the metal-oxide-semiconductor field-effect transistor (MOSFET or MOS transistor) that actually enabled all contemporary digital microelectronics, including computers, communications, microprocessors that are running everything from car engines to bread makers to planes, etc. It very well may be the most important invention¹³ of the 20th century that has formed the contemporary civilization as we know it. However, the MOSFET is a semiconductor-based nanodevice that has reached its top speed limit of ~ 100 GHz bandwidth, while much faster devices are presently demanded.

The spaser is the size of a MOSFET (~ 10 nm) but, based on metals, it is inherently faster, by a factor of 1000, as we have shown above in Sec. IV. Until now, the development of the SPASER has been hindered by the absence of its theory and the vision of the ways of its development. This necessarily must be quantum theory due to the quantum amplification mechanism which the spaser is based on. This paper has developed such a quantum theory of the spaser. It has given answers to the questions that are absolutely essential in fundamental research and applications of the spaser: What are physical foundations of the design and optimization of spaser? What does the threshold of spasing depend on? How to set a spaser in the mode of a bistable (logical) amplifier? What are the gain of this amplifier and the speed (bandwidth) of its ultrafast operations? Given in this article, the answers to these questions show that the spaser is potentially a high-gain, ultrafast (femtosecond) amplifier, generator, and dynamic memory nanodevice. Whether it will develop to become a nanoplasmonic counterpart of the MOSFET in the near future remains to be seen, but these results show a reasonable likelihood of such a development.

This work was supported by grants from the Chemical Sciences, Biosciences and Geosciences Division of the Office of Basic Energy Sciences, Office of Science, U.S. Department of Energy, a grant CHE-0507147 from NSF, and a grant from the US-Israel BSF. Work at Garching was supported under contract from Ludwig Maximilian University of Munich (Germany) in the framework of the Munich Advanced Photonics Center (MAP).

VI. METHODS

The SP eigenmodes $\varphi_n(\mathbf{r})$ are described by a wave equation (with homogeneous boundary conditions)^{4,17}

$$\nabla\Theta(\mathbf{r})\nabla\varphi_n(\mathbf{r}) = s_n\nabla^2\varphi_n(\mathbf{r}), \quad (8)$$

where n is the mode number, s_n is corresponding eigenvalue, and $\Theta(\mathbf{r})$ is the characteristic function equal to 1 for \mathbf{r} in the metal component and 0 in the dielectric.

Note that the eigenvalues s_n are all real and contained in the range $1 \geq s_n \geq 0$. The eigenmodes are normalized by an integral over the volume V of the system, $\int_V |\nabla\varphi_n(\mathbf{r})|^2 d^3r = 1$. The physical frequency ω_n of the SPs is defined by an equation $\text{Re}[s(\omega_n)] = s_n$, where $s(\omega) = \varepsilon_d / [\varepsilon_d - \varepsilon_m(\omega)]$ is Bergman's spectral parameter, ε_d is the permittivity of the ambient dielectric, and $\varepsilon_m(\omega)$ is the metal permittivity.

The electric field operator³⁸ of the quantized SPs is⁴

$$\mathbf{E}(\mathbf{r}) = -\sum_n A_n \nabla\varphi_n(\mathbf{r})(\hat{a}_n + \hat{a}_n^\dagger), \quad A_n = \left(\frac{4\pi\hbar s_n}{\varepsilon_d s'_n} \right)^{1/2}, \quad (9)$$

where \hat{a}_n^\dagger and \hat{a}_n are the SP creation and annihilation operators, and $s'_n = \text{Re}[ds(\omega_n)/d\omega_n]$.

The spaser Hamiltonian has the form

$$H = H_g + \hbar \sum_n \omega_n \hat{a}_n^\dagger \hat{a}_n - \sum_p \mathbf{E}(\mathbf{r}_p) \mathbf{d}^{(p)}, \quad (10)$$

where H_g is the Hamiltonian of the gain medium, p is an index (label) of a gain medium chromophore, \mathbf{r}_p is its coordinate vector, and $\mathbf{d}^{(p)}$ is its dipole moment operator. In this paper, we will treat the active medium quantum mechanically but the SPs quasiclassically, considering \hat{a}_n as a classical quantity (c-number) a_n with time dependence as $a_n = a_{0n} \exp(-i\omega t)$, where a_{0n} is a slowly-varying amplitude. The number of coherent SPs per spasing mode is then given by $N_p = |a_{0n}|^2$. This approximation neglects the quantum fluctuations of the SP amplitudes. However, when necessary, we will take into account these quantum fluctuations, in particular, to describe the spectrum of the spaser.

Introducing $\rho^{(p)}$ as the density matrix of a p th chromophore, we can find its equation of motion in a conventional way by commuting it with the Hamiltonian (10) as $i\hbar\dot{\rho}^{(p)} = [\rho^{(p)}, H]$, where the dot denotes temporal derivative. We will use the standard rotating wave approximation (RWA), which only takes into account the resonant interaction between the optical field and chromophores. We denote $|1\rangle$ and $|2\rangle$ as the ground and excited states of a chromophore, with the transition $|2\rangle \rightleftharpoons |1\rangle$ resonant to the spasing plasmon mode n . In this approximation, the time dependence of the nondiagonal elements of the density matrix is $(\rho^{(p)})_{12} = \bar{\rho}_{12}^{(p)} \exp(i\omega t)$, and $(\rho^{(p)})_{21} = \bar{\rho}_{12}^{(p)*} \exp(-i\omega t)$, where $\bar{\rho}_{12}^{(p)}$ is a time-independent amplitude defining the coherence (polarization) for the $|2\rangle \rightleftharpoons |1\rangle$ spasing transition in a p th chromophore of the gain medium.

Introducing a rate constant Γ_{12} to describe the polarization relaxation and a difference $n_{21}^{(p)} = \rho_{22}^{(p)} - \rho_{11}^{(p)}$ as the population inversion on this spasing transition, we derive an equation of motion for the non-diagonal element of the density matrix as

$$\dot{\bar{\rho}}_{12}^{(p)} = -[i(\omega - \omega_{12}) + \Gamma_{12}] \bar{\rho}_{12}^{(p)} + i n_{21}^{(p)} \Omega_{12}^{(a)*}, \quad (11)$$

where $\Omega_{12}^{(p)} = -A_n \mathbf{d}_{12}^{(p)} \nabla\varphi_n(\mathbf{r}_p) a_{0n} / \hbar$ is the Rabi frequency for the spasing transition in a p th chromophore,

and $\mathbf{d}_{12}^{(p)}$ is the corresponding transitional dipole element. Note that always $\mathbf{d}_{12}^{(p)}$ is either real or can be made real by a proper choice of the quantum state phases, making the Rabi frequency $\Omega_{12}^{(p)}$ also a real quantity.

An equation of motion for n_{21}^p can be found in a standard way by commutating it with H . To provide conditions for the population inversion ($n_{21}^p > 0$), we imply existence of a third level. For simplicity, we assume that it very rapidly decays into the excited state $|2\rangle$ of the chromophore, so its own populations is negligible. It is pumped by an external source from the ground state (optically or electrically) with some rate that we will denote g . In this way, we obtain the following equation of motion:

$$\dot{n}_{21}^{(p)} = -4\text{Im} \left[\bar{\rho}_{12}^{(p)} \Omega_{21}^{(p)} \right] - \gamma_2 \left(1 + n_{21}^{(p)} \right) + g \left(1 - n_{21}^{(p)} \right), \quad (12)$$

where γ_2 is the decay rate $|2\rangle \rightarrow |1\rangle$.

The stimulated emission of the SPs is described as their excitation by the coherent polarization of the gain medium. The corresponding equation of motion can be obtained using Hamiltonian (10) and adding the SP relaxation with a rate of γ_n as

$$\dot{a}_{0n} = [i(\omega - \omega_n) - \gamma_n] a_{0n} + i \sum_p \rho_{12}^{(p)*} \Omega^{(p)12}. \quad (13)$$

Another relevant process is spontaneous emission of SPs by a chromophore into a spasing SP mode. The corresponding rate $\gamma_2^{(p)}$ for a chromophore at a point \mathbf{r}_p can be found in a standard way using the quantized field (9) as

$$\gamma_2^{(p)} = 2 \frac{A_n^2}{\hbar \gamma_n} |\mathbf{d}_{12} \nabla \varphi_n(\mathbf{r}_p)|^2 \frac{(\Gamma_{12} + \gamma_n)^2}{(\omega_{12} - \omega_n)^2 + (\Gamma_{12} + \gamma_n)^2}. \quad (14)$$

As in Schawlow-Towns theory of laser-line width, this spontaneous emission of SPs leads to the diffusion of the

phase of the spasing state. This defines width γ_s of the spasing line as

$$\gamma_s = \frac{\sum_p \left(1 + n_{21}^{(p)} \right) \gamma_2^{(p)}}{2(2N_p + 1)}. \quad (15)$$

This width is small for a case of developed spasing when $N_p \gg 1$. However, for $N_p \sim 1$, the predicted width may be too high because the spectral diffusion theory assumes that $\gamma_s \lesssim \gamma_n$. To take into account this limitation in a simple way, we will interpolate to find the resulting spectral width Γ_s of the spasing line as $\Gamma_s = (\gamma_n^{-2} + \gamma_s^{-2})^{-1/2}$.

We will also examine the spaser as a logical amplifier. One of the ways to set the spaser in such a mode is to add a saturable absorber. This is described by the same Eqs. (11)-(13) where the chromophores belonging to the absorber are not pumped by the external source directly, i.e., for them in Eq. (12) one has to set $g = 0$.

Numerical examples are given for a silver nanoshell where the core and the external dielectric have the same permittivity of $\varepsilon_d = 2$; the permittivity of silver is adopted from Ref. 37. The following realistic parameters of the gain medium are used (unless indicated otherwise): $d_{12} = 1.5 \times 10^{-17}$ esu, $\hbar \Gamma_{12} = 10$ meV, $\gamma_2 = 4 \times 10^{12}$ s $^{-1}$ (this value takes into account the spontaneous decay into SPs), and density of the gain medium chromophores is $\rho = 2.4 \times 10^{20}$ cm $^{-3}$, which is realistic for dye molecules but may be somewhat high for semiconductor quantum dots that were proposed as the chromophores⁴ and used in experiments¹⁹. We will assume a dipole SP mode and chromophores situated in the core of the nanoshell as shown in Fig. 1 (d). This configuration are of advantage both functionally (because the region of the high local fields outside the shell is accessible for various applications) and computationally (the uniformity of the modal fields makes the summation of the chromophores trivial, thus greatly facilitating numerical procedures).

* Electronic address: mstockman@gsu.edu;
URL: <http://www.phy-astr.gsu.edu/stockman>

¹ L. Novotny and B. Hecht, *Principles of Nano-Optics* (Cambridge University Press, Cambridge, New York, 2006).

² * M. I. Stockman, M. F. Kling, U. Kleineberg, and F. Krausz, *Nature Photonics* **1**, 539 (2007).

³ M. I. Stockman, *New J. Phys.* **10**, 025031 (2008).

⁴ D. J. Bergman and M. I. Stockman, *Phys. Rev. Lett.* **90**, 027402 (2003).

⁵ H. A. Atwater, *Sci. Am.* **296**, 56 (2007).

⁶ J. N. Anker, W. P. Hall, O. Lyandres, N. C. Shah, J. Zhao, and R. P. V. Duyne, *Nature Materials* **7**, 442 (2008).

⁷ A. Israel, M. Mrejen, Y. Lovsky, M. Polhan, S. Maier, and A. Lewis, *Laser Focus World* **43**, 99 (2007).

⁸ L. Tang, S. E. Kocabas, S. Latif, A. K. Okyay, D. S. Lygagnon, K. C. Saraswat, and D. A. B. Miller, *Nat. Phot.*

2, 226 (2008).

⁹ W. A. Challener, C. Peng, A. V. Itagi, D. Karns, W. Peng, Y. Peng, X. Yang, X. Zhu, N. J. Gokemeijer, Y. T. Hsia, et al., *Nat. Phot.* **3**, 220 (2009).

¹⁰ S. Kim, J. H. Jin, Y. J. Kim, I. Y. Park, Y. Kim, and S. W. Kim, *Nature* **453**, 757 (2008).

¹¹ N. Nagatani, R. Tanaka, T. Yuhi, T. Endo, K. Kerman, and Y. T. and. E Tamiya, *Science and Technology of Advanced Materials* **7**, 270 (2006).

¹² L. R. Hirsch, R. J. Stafford, J. A. Bankson, S. R. Sershen, B. Rivera, R. E. Price, J. D. Hazle, N. J. Halas, and J. L. West, *Proc. Natl. Acad. Sci. USA* **100**, 13549 (2003).

¹³ D. Kahng, *United States Patent* 3,102,230 (1963).

¹⁴ Y. Tsidis, *Operation and Modeling of the MOS Transistor* (McGraw-Hill, New York, 1999).

¹⁵ M. I. Stockman, *Nat. Phot.* **2**, 327 (2008).

¹⁶ M. T. Hill, Y.-S. Oei, B. Smalbrugge, Y. Zhu, T. d. Vries,

- P. J. v. Veldhoven, F. W. M. v. Otten, T. J. Eijkemans, J. a. P. Turkiewicz, H. d. Waardt, et al., *Nat. Phot.* **1**, 589 (2007).
- ¹⁷ M. I. Stockman, S. V. Faleev, and D. J. Bergman, *Phys. Rev. Lett.* **87**, 167401 (2001).
- ¹⁸ I. A. Larkin and M. I. Stockman, *Nano Lett.* **5**, 339 (2005).
- ¹⁹ E. Plum, V. A. Fedotov, P. Kuo, D. P. Tsai, and N. I. Zheludev, *Opt. Expr.* **17**, 8548 (2009).
- ²⁰ J. Seidel, S. Grafstroem, and L. Eng, *Phys. Rev. Lett.* **94**, 177401 (2005).
- ²¹ M. A. Noginov, G. Zhu, M. Mayy, B. A. Ritzo, N. Noginova, and V. A. Podolskiy, *Phys. Rev. Lett.* **101**, 226806 (2008).
- ²² K. Li, X. Li, M. I. Stockman, and D. J. Bergman, *Phys. Rev. B* **71**, 115409 (2005).
- ²³ Z. G. Dong, H. Liu, T. Li, Z. H. Zhu, S. M. Wang, J. X. Cao, S. N. Zhu, and X. Zhang, *Opt. Expr.* **16**, 20974 (2008).
- ²⁴ M. Wegener, J. L. Garcia-Pomar, C. M. Soukoulis, N. Meinzer, M. Ruther, and S. Linden, *Opt. Expr.* **16**, 19785 (2008).
- ²⁵ J. A. Gordon and R. W. Ziolkowski, *Opt. Expr.* **15**, 2622 (2007).
- ²⁶ A. K. Sarychev and G. Tartakovsky, *Phys. Rev. B* **75**, 085436 (2007).
- ²⁷ Z. H. Zhu, H. Liu, S. M. Wang, T. Li, J. X. Cao, W. M. Ye, X. D. Yuan, and S. N. Zhu, *Appl. Phys. Lett.* **94**, 103106 (2009).
- ²⁸ N. I. Zheludev, S. L. Prosvirnin, N. Papasimakis, and V. A. Fedotov, *Nat. Phot.* **2**, 351 (2008).
- ²⁹ M. Ambati, S. H. Nam, E. Ulin-Avila, D. A. Genov, G. Bartal, and X. Zhang, *Nano Lett.* **8**, 3998 (2008).
- ³⁰ Z. K. Zhou, X. R. Su, X. N. Peng, and L. Zhou, *Opt. Expr.* **16**, 18028 (2008).
- ³¹ M. A. Noginov, V. A. Podolskiy, G. Zhu, M. Mayy, M. Bahoura, J. A. Adegoke, B. A. Ritzo, and K. Reynolds, *Opt. Expr.* **16**, 1385 (2008).
- ³² M. A. Noginov, G. Zhu, M. Bahoura, J. Adegoke, C. Small, B. A. Ritzo, V. P. Drachev, and V. M. Shalaev, *Appl. Phys. B* **86**, 455 (2007).
- ³³ M. A. Noginov, *J. Nanophotonics* **2**, 021855 (2008).
- ³⁴ A. M. Belgrave, G. Zhu, N. Noginova, V. I. Gavrilenko, E. Herz, U. Wiesner, R. Bakker, V. P. Drachev, V. M. Shalaev, V. A. Podolskiy, et al., in *OSA Optics & Photonics Congress: Plasmonics and Metamaterials (META)* (Optical Society of America, Washington, DC, 2008).
- ³⁵ M. A. Noginov, in *NanoMeta 2009* (European Physical Society, Seefeld, Tirol, Austria, 2009), vol. 33A, p. Paper No THU5o.2.
- ³⁶ M. A. Noginov, G. Zhu, A. M. Belgrave, R. Bakker, V. M. Shalaev, E. E. Narimanov, S. Stout, E. Herz, T. Suteewong, and U. Wiesner, *Nature advance online publication*; <http://dx.doi.org/10.1038/nature08318> (2009).
- ³⁷ P. B. Johnson and R. W. Christy, *Phys. Rev. B* **6**, 4370 (1972).
- ³⁸ Note that we have corrected a misprint in Ref. 4 replacing in the coefficient 2π by 4π .